drugs and drug candidates

MDPI

Article

Design of a First-in-Class homoPROTAC to Induce ICP0 Degradation in Human Herpes Simplex Virus 1

Leyla Salimova [1], Ali Sahin [2], Ozge Ardicli [3], Fatima Hacer Kurtoglu Babayev [4], Zeynep Betul Sari [5,6], Muhammed Emin Sari [7], Muhammet Guzel Kurtoglu [8], Sena Ardicli [9,*] and Huseyn Babayev [10,*]

1 Department of Biotechnology, Faculty of Biology, Baku State University, Baku 1148, Azerbaijan; salimova.leyla.amil@bsu.edu.az
2 Department of Urology, Faculty of Medicine, Selcuk University, 42130 Konya, Türkiye; sahin@silicosome.com
3 Division of Food Processing, Milk and Dairy Products Technology Program, Karacabey Vocational School, Bursa Uludag University, 16700 Bursa, Türkiye; ozgeyilmaz@uludag.edu.tr
4 Institute for Vascular Signalling, Centre for Molecular Medicine, Goethe University, 60590 Frankfurt am Main, Germany; kurtoglu@vrc.uni-frankfurt.de
5 Department of Medical Biology, Faculty of Medicine, Ankara Yildirim Beyazit University, 06690 Ankara, Türkiye; zeynepbetulsari@aybu.edu.tr
6 Yenimahalle Training and Research Hospital, Department of Medical Biology, Ankara Yildirim Beyazit University, 06370 Ankara, Türkiye
7 Faculty of Medicine, Department of Medical Biology, Necmettin Erbakan University, 42090 Konya, Türkiye; sari@silicosome.com
8 Department of Medical Microbiology, Faculty of Medicine, Bolu Abant Izzet Baysal University, 14280 Bolu, Türkiye; kurtoglumg@gmail.com
9 Department of Genetics, Faculty of Veterinary Medicine, Bursa Uludag University, 16059 Bursa, Türkiye
10 Swiss Institute of Allergy and Asthma Research (SIAF), University of Zurich, 7265 Davos, Switzerland
* Correspondence: sardicli@uludag.edu.tr (S.A.); huseyn.babayev@siaf.uzh.ch (H.B.); Tel.: +90-541-487-5448 (S.A.); +41-767-785-496 (H.B.)

Abstract

Background/Objectives: Human Herpes Simplex Virus 1 (HSV-1) is a common pathogen that establishes lifelong latent infections. The emergence of drug resistance necessitates novel therapeutic strategies. This study introduces a novel antiviral approach: a bivalent degrader designed to induce the degradation of an essential protein. **Methods**: A structural model of ICP0, generated via the Chai-1 AI platform, was analyzed with fpocket, P2Rank, and KVFinder to identify a superior allosteric target site. An iterative de novo design workflow with CReM-dock then yielded a lead scaffold based on its predicted affinity and drug-like properties. This selected "warhead" was used to rationally design the final bivalent degrader, ICP0-deg-01, for the ICP0 dimer model. **Results**: The generative process yielded a lead chemical scaffold that was selected based on its predicted binding affinity and favorable drug-like properties. This scaffold was used to rationally design a single candidate bivalent degrader, ICP0-deg-01. Our structural model predicts that ICP0-deg-01 can successfully bridge two ICP0 protomers, forming an energetically favorable ternary complex. **Conclusions**: This work provides a computational proof-of-concept for a novel class of anti-herpetic agents and identifies a lead candidate for future molecular dynamics simulations and experimental validation.

Keywords: herpes simplex; proteolysis-targeting chimeras; homoPROTAC; ICP0; virus latency; drug design; ubiquitin–protein ligases

check for updates

Academic Editors: Osvaldo Andrade Santos-Filho and Jean Jacques Vanden Eynde

Received: 8 July 2025
Revised: 12 August 2025
Accepted: 2 September 2025
Published: 8 September 2025

Citation: Salimova, L.; Sahin, A.; Ardicli, O.; Kurtoglu Babayev, F.H.; Sari, Z.B.; Sari, M.E.; Kurtoglu, M.G.; Ardicli, S.; Babayev, H. Design of a First-in-Class homoPROTAC to Induce ICP0 Degradation in Human Herpes Simplex Virus 1. *Drugs Drug Candidates* **2025**, *4*, 42. https://doi.org/10.3390/ddc4030042

Copyright: © 2025 by the authors. Licensee MDPI, Basel, Switzerland. This article is an open access article distributed under the terms and conditions of the Creative Commons Attribution (CC BY) license (https://creativecommons.org/licenses/by/4.0/).

1. Introduction

Human Herpes Simplex Virus 1 (HSV-1) is a persistent challenge to public health [1,2]. This ubiquitous pathogen has infected a majority of the global population, causing a wide spectrum of clinical diseases that extend far beyond simple cold sores [1,2]. Its manifestations include painful and recurrent oral lesions, potentially blinding herpetic keratitis, and life-threatening encephalitis, with high morbidity in neonates and immunocompromised individuals [3]. Beyond the physical symptoms, the virus imposes a significant psychological burden due to its lifelong persistence and the unpredictable nature of its reactivation [4,5]. At the core of this challenge is the virus's ability to establish a state of latency, hiding as a silent episome within the nuclei of sensory neurons, completely shielded from both the host immune system and current antiviral therapies [6,7].

The development of nucleoside analogs, with acyclovir as the prototype, marked a revolutionary advance in the management of HSV infections [8,9]. These drugs function as chain terminators for the viral DNA polymerase, effectively halting viral replication during active lytic cycles [10,11]. The clinical success of this drug class in controlling the severity and duration of recurrent episodes is undeniable. However, the efficacy of this drug class is limited [12,13]. The fundamental limitation of these drugs is their complete inability to target the latent viral reservoir, meaning they can manage symptoms but can never provide a cure [14,15]. Furthermore, decades of clinical use have led to the inevitable emergence of drug-resistant viral strains, particularly in immunocompromised patients, where mutations in the viral thymidine kinase or DNA polymerase render the drugs ineffective [16]. This combination of an inaccessible latent reservoir and growing drug resistance creates a clear and urgent unmet medical need for a new generation of anti-herpetic agents that operate through entirely novel mechanisms of action.

In recent years, the field of drug discovery has been transformed by the rise in targeted protein degradation (TPD) [17]. This innovative modality seeks not just to inhibit a target protein, but to eliminate it from the cell entirely [17,18]. The flagship technology of TPD is the proteolysis-targeting chimera (PROTAC), a bifunctional molecule designed to hijack the cell's own quality control machinery, the ubiquitin–proteasome system (UPS) [17,19]. By simultaneously binding a protein of interest (POI) and a cellular E3 ubiquitin ligase—one of over 600 enzymes responsible for substrate recognition within the UPS—a PROTAC induces the formation of a temporary ternary complex [19,20]. This induced proximity enables the E3 ligase to tag the POI with a polyubiquitin chain, marking it for destruction by the proteasome. The catalytic nature of this process, where one PROTAC molecule can trigger the degradation of many target molecules, has established TPD as a powerful therapeutic strategy, with several PROTACs now advancing through clinical trials for cancer and other diseases [17].

While TPD has proven its value against human protein targets, its application to infectious diseases, particularly virology, represents a new and exciting frontier. The concept of degrading an essential viral protein, rather than merely blocking its active site, is therapeutically compelling and could lead to more profound and durable antiviral effects [21,22]. This study aims to forge a path in this direction by targeting Infected Cell Protein 0 (ICP0) of HSV-1, an essential viral regulatory protein. As an immediate-early (IE) protein, ICP0 is one of the very first viral products to appear, and it immediately executes a multi-pronged assault to dismantle cellular defenses [23,24]. Its power is derived from its function as a C3HC4 RING finger E3 ubiquitin ligase that efficiently targets host proteins [24–26]. ICP0's "hit list" comprises a strategic collection of proteins central to the host's antiviral response [27,28].

The viral protein ICP0 acts as a central hub that disrupts host cell defenses by targeting key proteins across multiple immunity pathways. To counteract intrinsic immunity, ICP0 targets components of the DNA damage response, including RNF168, RNF8, and DNA-PKcs. It also dismantles innate immunity by interfering with the interferon response and

NF-κB signaling. Specifically, it targets IκBα, as well as the TLR signaling adaptors MyD88 and Mal, which ultimately suppresses inflammatory mechanisms. A primary function of ICP0 is the disruption of ND10 nuclear bodies by targeting their core components PML, Sp100, and IFI16. This action overcomes viral genome silencing and promotes viral transcription. Additionally, ICP0 interacts with USP7, which leads to its own destabilization and further suppresses TLR and NF-κB signaling [29] (Figure A1).

Given its absolute centrality to viral pathogenesis, ICP0 is an outstanding therapeutic target. This study puts forth a novel strategy to neutralize it: the design of a first-in-class homoPROTAC. This molecule is engineered with identical warheads designed to bind to same allosteric site on the ICP0 protein. Our central hypothesis is that this bivalent binding will leverage the natural tendency of ICP0 to self-associate via its C-terminal dimerization domain [23], inducing the formation of a stable ICP0–homoPROTAC–ICP0 ternary complex. Within this enforced dimer, the potent E3 ligase domain of one ICP0 molecule will be ideally positioned to catalyze the ubiquitination and subsequent degradation of its partner. This "viral self-destruction" approach is fundamentally different from conventional PROTACs as it obviates the need to recruit a host E3 ligase, which may improve its specificity for infected cells (Figure 1). The objective of this work is to provide the first computational proof-of-concept for this strategy, employing a sophisticated pipeline of AI-driven drug design tools to rationally design and validate these novel antiviral agents.

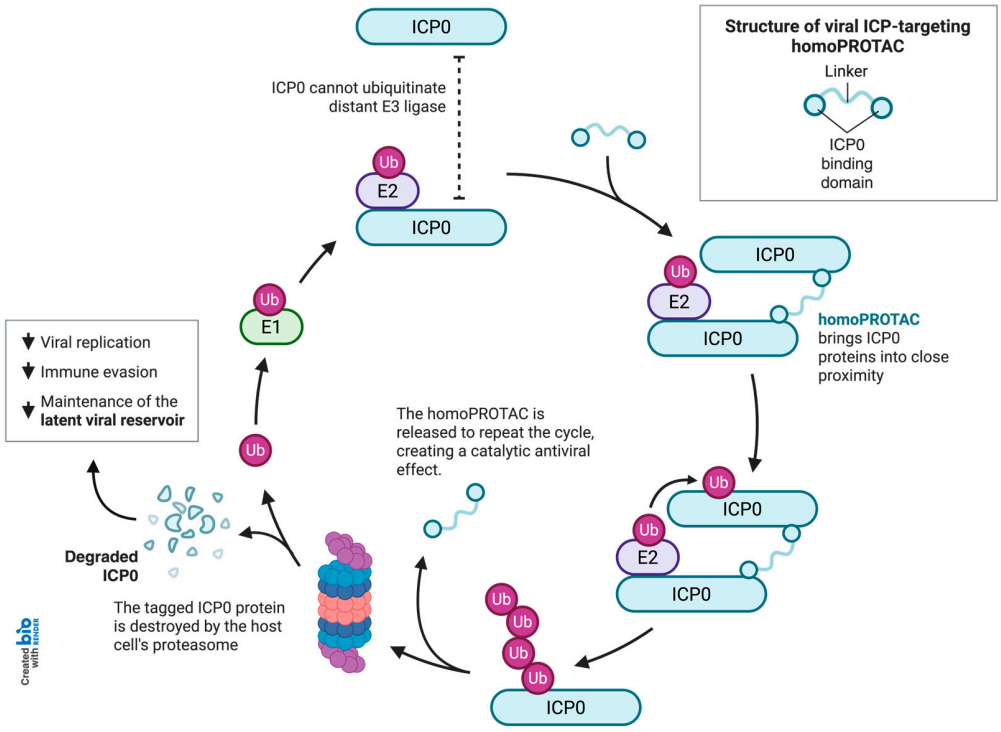


Figure 1. The proposed 'viral self-destruction' mechanism of an ICP0-targeting homoPROTAC. The figure illustrates the catalytic cycle of a bivalent degrader designed to induce the self-destruction of the essential Herpes Simplex Virus 1 (HSV-1) E3 ligase, ICP0. The cycle begins when ubiquitin (Ub) is activated by a host E1 enzyme and transferred to an E2 conjugating enzyme, which then binds to ICP0. A homoPROTAC molecule, composed of two ICP0-binding domains connected by a flexible linker, forces two ICP0 proteins into close proximity. This induced dimerization allows one ICP0 molecule to catalyze the transfer of Ub from the E2 enzyme onto its partner. Repeated ubiquitination results in a polyubiquitin chain, marking the viral protein for destruction. The tagged ICP0 is then degraded by the host cell's proteasome. The degradation of ICP0 is predicted to have a potent antiviral effect by inhibiting viral replication, preventing immune evasion, and disrupting the maintenance of the latent viral reservoir. The homoPROTAC is then released and is free to repeat the cycle, creating a catalytic antiviral effect.

2. Results

2.1. ICP0 Structural Analysis Reveals a Superior Druggable Pocket for Bivalent Ligand Design

To establish a reliable three-dimensional structure for ICP0, a comparative analysis of models from multiple state-of-the-art AI platforms, including AlphaFold 3 and RoseTTAFold2, was performed (Figure 2A). While these other tools were used for comparison and to build confidence in the overall fold, the Chai-1 model with explicitly modeled zinc ions was selected as the definitive structure for all subsequent computational applications (Figure 2B). The selected Chai-1 model yielded a predicted TM-score (pTM) of 0.26 and an interface pTM (ipTM) of 0.12. This low global confidence is largely attributable to the presence of extensive random coils, corresponding to predicted intrinsically disordered regions in the full-length protein. However, the functionally critical region encompassing the RING finger domain (residues 110–200) was consistently predicted with high local confidence across all models, validating its structural integrity for further analysis. Specifically, this region yielded a mean predicted Local Distance Difference Test (pLDDT) score of 66.6, substantially higher than the 46.9 average for the full-length protein (Figure A2).

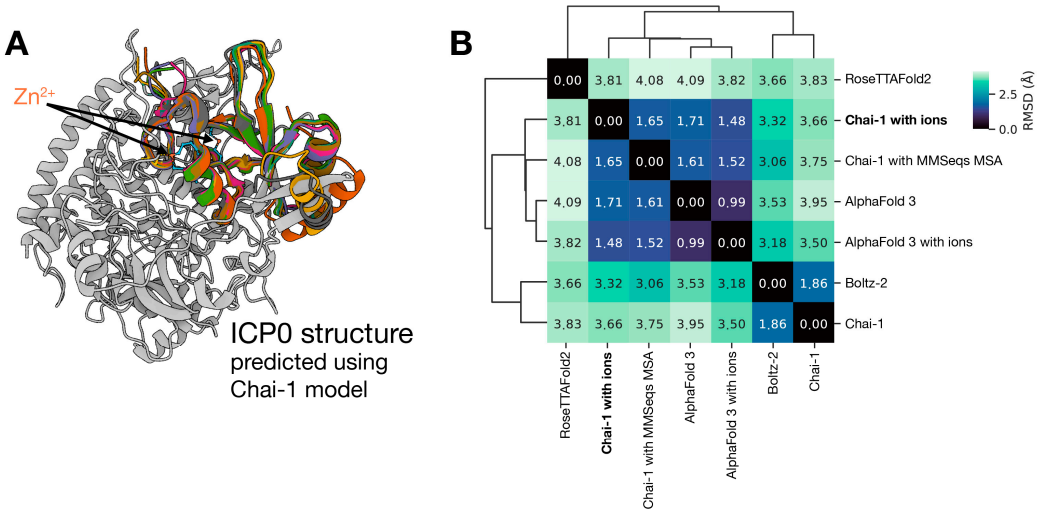


Figure 2. (**A**) The final full-length Chai-1 consensus model of ICP0 selected for this study is shown as a gray ribbon. To visually demonstrate the high structural agreement in the domain of interest, the truncated region corresponding to residues 110–200 from the other AI models is overlaid in various colors, showing excellent structural overlap. The explicitly modeled zinc (Zn^{2+}) ions in the RING finger domain are also indicated. (**B**) The matrix shows the pairwise Root Mean Square Deviation (RMSD, in Ångstroms) between seven different full-length ICP0 structural models generated by various AI platforms. The low RMSD values indicate a high degree of structural consensus among the top-performing models.

Subsequent druggability analysis performed on this Chai-1 model identified several potential binding cavities on the protein surface. A quantitative comparison revealed that one of these sites was vastly superior, exhibiting the highest druggability score (0.215) and the largest volume (617 $Å^3$) (Table 1). This single, high-quality pocket, visualized in Figure 3A, was consequently selected as the exclusive target for all subsequent hit generation and degrader design efforts.

Table 1. Quantitative analysis of predicted druggable pockets on ICP0. The table details the key physicochemical properties of the top four pockets identified. Pocket 2 was selected as the exclusive target based on its superior druggability score and volume.

Property	Pocket 1	Pocket 2 (Target)	Pocket 3	Pocket 4
Druggability Score	0.115	0.215	0.008	0.001
Volume (Å^3)	303.173	617.16	249.952	290.706
Number of Alpha Spheres	35	59	16	17
Total SASA (Å^2)	98.302	197.97	80.75	87.032
Apolar SASA (Å^2)	71.25	130.424	73.249	59.174

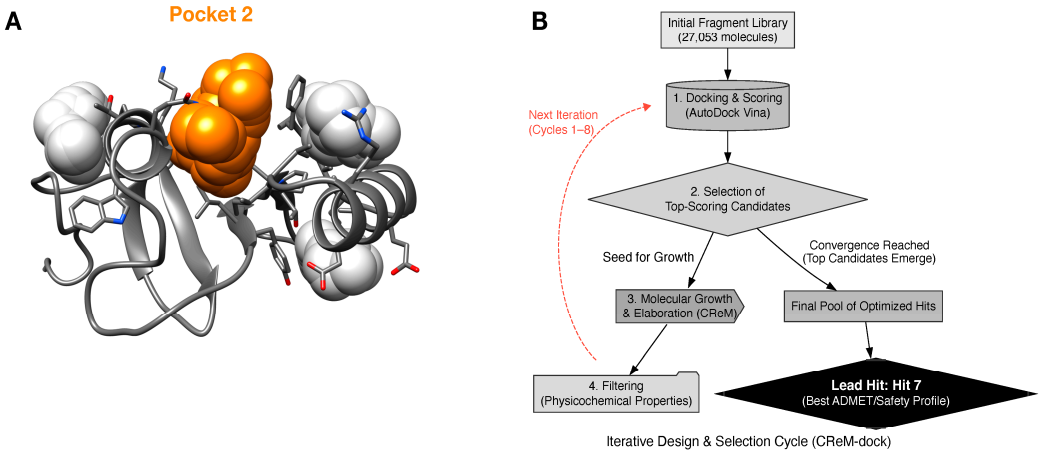


Figure 3. (**A**) Visualization of the superior druggable pocket on ICP0. The AI-predicted structure of ICP0 is shown as a gray ribbon. The single pocket selected for the bivalent degrader strategy (Pocket 2) is highlighted with an orange surface, illustrating its size and location. (**B**) A schematic of the iterative CReM-dock workflow used for hit identification. The process starts with an initial library of 27,053 small molecules and proceeds through cycles of docking, selection, molecular growth, and filtering, ultimately converging on the final lead hit scaffold, Hit 7.

2.2. Virtual Screening Identifies High-Affinity Core Scaffolds

The de novo design of novel scaffolds was conducted using an iterative CReM-dock workflow that completed 8 cycles of molecular docking, generation, and filtering (Figure 3B). The screening began with an initial library of 27,053 small molecules. In the first iteration, this pool was docked, and the best candidates were elaborated, massively expanding the chemical space to over 124,000 new molecules that passed physicochemical filters.

Over the following seven iterations, the process computationally evaluated and refined this chemical space. The number of candidate molecules was progressively focused down, from the initial expansion to 26,793 candidates in iteration 2, then to 1606 in iteration 3, and ultimately to a final pool of 73 molecules entering the last cycle. In total, approximately 182,000 unique docking calculations were performed throughout the campaign. The generative process automatically concluded after the eighth iteration when no further valid chemical elaborations could be produced from the remaining candidates, indicating that the algorithm had reached convergence.

From the final pool of high-scoring molecules generated by this extensive campaign, the top candidates were subjected to a rigorous ADMET and physicochemical analysis to identify the single most promising scaffold for elaboration (Table 2). Based on this comprehensive assessment, Hit 7 was selected as the lead scaffold, primarily due to its superior predicted aqueous solubility and its minimal predicted inhibition of cytochrome P450 enzymes.

Table 2. Predicted physicochemical and ADMET properties of the top 10 hit scaffolds. The table details the key predicted properties for the top 10 hit scaffolds resulting from the iterative CReM-dock design campaign. This multi-parameter analysis, including molecular weight (MW), lipophilicity (Consensus LogP), aqueous solubility (ESOL LogS), potential for cytochrome P450 (CYP) enzyme inhibition, and synthetic accessibility (SA Score), was used to select a single lead candidate for elaboration into the final bivalent degrader. Hit 7 was selected based on its optimal balance of these properties, most notably its superior predicted solubility and minimal CYP inhibition profile.

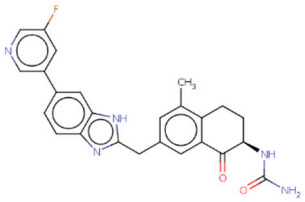
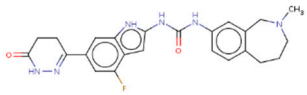
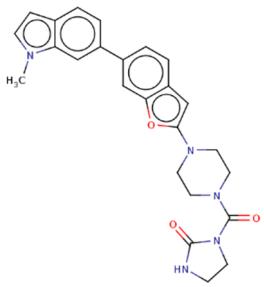
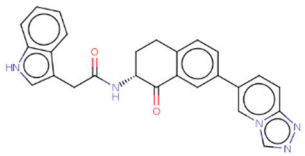
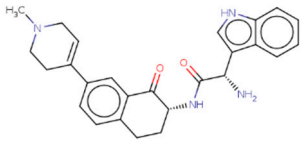
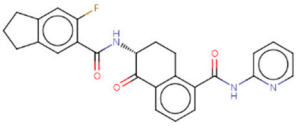
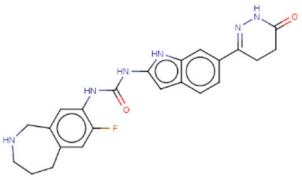
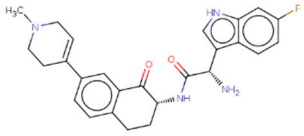
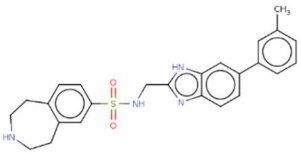
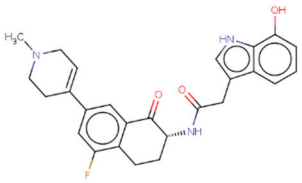
Hits	Structure	Predicted Affinity (kcal/mol)	MW (Da)	Consensus LogP	ESOL LogS	Predicted CYP Inhibition	SA Score
Hit 1		−10.887	443.47	3.41	−4.9	1A2, 2C19, 2C9, 3A4	3.66
Hit 2		−10.758	448.49	2.96	−4.06	1A2, 2D6	3.78
Hit 3		−10.743	443.5	2.72	−4.71	2C19, 2C9, 2D6, 3A4	3.65
Hit 4		−10.677	435.48	3.34	−5.31	1A2, 2C19, 2C9, 2D6, 3A4	3.66
Hit 5		−10.61	428.53	2.75	−4.15	2C19, 2C9, 3A4	4.36
Hit 6		−10.608	443.47	3.85	−5.22	1A2, 2C19, 2C9, 2D6, 3A4	3.64
Hit 7		−10.557	434.47	2.73	−3.69	1A2	3.62
Hit 8		−10.462	446.52	3.06	−4.31	2C19, 2D6, 3A4	4.44

Table 2. *Cont.*

Hits	Structure	Predicted Affinity (kcal/mol)	MW (Da)	Consensus LogP	ESOL LogS	Predicted CYP Inhibition	SA Score
Hit 9		−10.433	446.56	3.55	−5.18	1A2, 2D6, 3A4	3.39
Hit 10		−10.431	447.5	3.34	−4.61	2C19, 2C9, 3A4	4.16

2.3. Rational Design of the Lead Bivalent Degrader ICP0-deg-01

Using the lead scaffold Hit 7 as the exclusive "warhead," a single, final bivalent degrader—designated ICP0-deg-01—was rationally designed. This was achieved by docking two copies of the Hit 7 warhead into the identical target sites of the ICP0 dimer model and computationally connecting them with a 16-carbon alkyl linker.

The resulting ternary complex model showed how ICP0-deg-01 effectively bridges the two ICP0 protomers (colored orange and green) at the dimer interface. As shown in the detailed interaction map (Figure 4A), each "Hit 7" warhead is deeply anchored within its respective pocket through a network of favorable interactions. These include key hydrogen bonds with the side chain of Glu112, as well as extensive hydrophobic contacts with residues such as Ile140, Val165, and Val167. The flexible 16-carbon linker successfully spanned the distance between the two bound warheads, creating a stable, bridged structure evaluated as the lead candidate for this study (Figure 4B). The predicted physicochemical and ADMET properties of this final candidate are detailed in the Appendix A (Table A1).

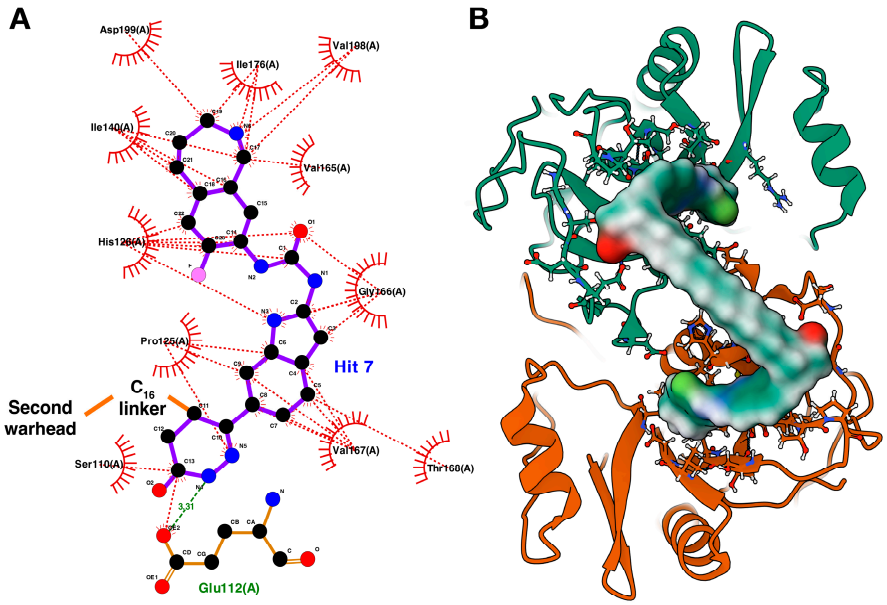


Figure 4. (**A**) Predicted binding mode of lead scaffold Hit 7 in the ICP0 dimer. A 2D diagram detailing the key molecular interactions between Hit 7 and the ICP0 binding pocket. The ligand is shown with black (carbon), blue (nitrogen), red (oxygen), and pink (fluorine) atoms connected by purple covalent bonds. Hydrogen bonds are shown as dashed green lines, and residues involved in hydrophobic interactions are depicted with red arcs and dashed red lines. The attachment point of the 16-carbon

linker leading to the second warhead is shown with orange lines. (**B**) 3D representation of the docked pose of ICP0-deg-01 (surface model) based on Hit 7 at the interface of the ICP0 dimer. The two protomers of ICP0 are shown as green and orange ribbons, with key interacting residues displayed as stick models.

3. Discussion

This in silico study presents a rational computational strategy for the design of a first-in-class homoPROTAC against the essential HSV-1 protein, ICP0. By integrating state-of-the-art AI-driven structure prediction with a generative molecular design workflow, we identified a novel, superior druggable pocket on ICP0. This led to the identification of a lead hit scaffold, Hit 7, and the subsequent design of a single bivalent degrader candidate, ICP0-deg-01. Our structural model provides a basis for the hypothesis that ICP0-deg-01 can effectively bridge two ICP0 protomers, supporting the proposed "viral self-destruction" mechanism.

The strategic selection of ICP0 as the target is central to the therapeutic hypothesis. As a key regulator of the infectious cycle, the degradation of ICP0 is expected to severely impair the virus ability to counteract host defenses and replicate [30]. An important implication of this strategy is its potential to address the challenge of viral latency. A growing body of evidence suggests that latency is a dynamic state maintained by low-level, intermittent ICP0 expression [31]. Therefore, a therapeutic agent capable of eliminating the ICP0 protein could potentially disrupt the maintenance of the latent reservoir, preventing reactivation—a goal that has remained elusive for current antiviral therapies.

The "viral self-destruction" model itself offers significant advantages. By hijacking the viral E3 ligase to degrade itself, the mechanism is inherently specific to infected cells expressing ICP0, promising a wide therapeutic window. This novel mechanism of action is also critically important for combating the emergence of drug resistance that plagues current treatments like acyclovir. Our study moves beyond simple inhibition to propose a catalytic method of viral protein elimination.

Our computational workflow highlights the power of modern drug design tools. The iterative CReM-dock process was highly effective, exploring a vast chemical space through approximately 182,000 docking calculations over 8 iterations to identify novel scaffolds. The subsequent selection of Hit 7 was a deliberate, multi-parameter optimization, balancing a strong predicted binding affinity with a superior ADMET/safety profile. The final structural model of the ICP0-deg-01 ternary complex provides a detailed hypothesis for how this induced dimerization is achieved. The model predicts that the Hit 7 warheads are anchored by a network of specific hydrogen bonds and hydrophobic interactions, while the 16-carbon linker is of sufficient length to bridge the two protomers in an energetically favorable conformation.

The use of a single, non-optimized alkyl linker represents a significant simplification. The linker is now understood to be a critical component that governs a degrader's success, not merely a passive spacer. Its specific length, chemical makeup, and rigidity directly dictate the geometry and stability of the induced ternary complex, which in turn determines the efficiency of protein degradation [32]. Furthermore, the linker's properties have a profound impact on the molecule's overall drug-like characteristics, including its solubility, cell permeability, and metabolic stability. A comprehensive follow-up study would therefore require the systematic exploration of a linker library to optimize these parameters for the highest possible therapeutic effect.

While this study provides a computational proof-of-concept, its significant limitations must be clearly acknowledged. The most fundamental weakness is the study's reliance on an AI-generated structural model, particularly for the dimer interface that is central to the proposed mechanism. Furthermore, the absence of molecular dynamics simulations means that the stability and dynamic behavior of the final complex are purely hypothetical.

The therapeutic design was also simplified, using only a single hit scaffold and a single, non-optimized 16-carbon linker where a more comprehensive study would have explored a wider chemical space. The predicted ADMET profile of the final candidate shows several liabilities in molecular weight and solubility that are typical for first-generation degraders and underscore the need for future optimization (see Appendix A, Table A1). The entire study is computational, and all findings require rigorous experimental validation to be substantiated.

4. Materials and Methods

4.1. ICP0 Sequence Acquisition and AI-Driven Structural Prediction

The canonical protein sequence for Human Herpes Simplex Virus 1 (strain 17) ICP0 was acquired from the UniProt Knowledgebase (UniProt ID: P08393) [33]. As no complete experimental structure exists, a comprehensive in silico modeling approach was undertaken. A diverse pool of three-dimensional (3D) models of the full-length 775-amino acid protein was generated using multiple state-of-the-art AI-driven protein structure prediction platforms: AlphaFold-3 [34], Boltz-2 [35], Chai-1 [36], Protenix [37], and RoseTTAFold2 [38]. Notably, models from the AlphaFold Server and its derivatives were intentionally excluded from our workflow. This decision was made to ensure full compliance with its terms of use, which restricts the use of its output in conjunction with automated docking programs like AutoDock Vina, a key component of our study. From this pool, a final consensus model was selected by prioritizing models with both a high mean predicted Local Distance Difference Test (pLDDT) score and, critically, a chemically correct and functionally competent C3HC4 RING finger domain [24]. This involved meticulous validation of the coordination geometry of the two explicitly modeled zinc (Zn^{2+}) ions with the surrounding Cys/His residues. While the catalytic C3HC4 RING finger domain is defined as residues 116–156, we selected a larger fragment (residues 110–200) for all subsequent analyses. This expanded boundary was chosen to fully incorporate the functional domain and to account for the potential influence of adjacent, flexible regions on ligand accessibility and binding.

4.2. Druggability Analysis and Site Selection

To enable the bivalent degrader strategy, the selected ICP0 model was intensively analyzed to identify the most suitable druggable binding pocket. While initial interest was focused on the catalytic RING domain, analysis of the full-length model revealed more promising allosteric sites. The entire structure was subjected to a rigorous computational pipeline using three independent pocket detection algorithms: fpocket 4.0, P2Rank 2.3, and KVFinder 3.0. These algorithms generated quantitative metrics (e.g., Druggability Score, Volume, Polarity) for all potential cavities. Based on a consensus of these metrics, one particular pocket was identified as having a vastly superior druggability score and volume, making it the ideal candidate for binding a small molecule warhead and for mediating dimerization. This pocket was selected for the subsequent virtual screening.

4.3. Small Molecule Library Preparation

To construct a high-quality library suitable for virtual screening, a comprehensive collection of small molecules was assembled and meticulously refined. The foundation of this library was built upon three distinct sources. The first was the entirety of the DrugBank database, which was initially filtered to retain all carbon-containing molecules with a molecular mass exceeding 50 Daltons. This was augmented with a curated set of sp^3-rich small molecules from the CReM database and a specialized subset of the ChEMBL database (version 22), which was pre-filtered for a low heavy atom count.

Following aggregation, this composite library was subjected to a rigorous computational filtering cascade designed to ensure the selection of synthetically feasible and

medicinally relevant starting points. The chemical space was first constrained to molecules composed exclusively of common organic elements, namely carbon, nitrogen, oxygen, sulfur, phosphorus, and the halogens fluorine, chlorine, bromine, and iodine. To focus on small starting scaffolds suitable for screening, a stringent upper limit of 12 heavy atoms per molecule was imposed. Furthermore, to prioritize compounds amenable to straightforward chemical synthesis, a maximum synthetic accessibility (SA) score of 2.5 was enforced. As a final quality control measure, the library was purified of known promiscuous binders, nuisance compounds, and reactive functionalities by removing any molecule that triggered an alert from a suite of well-established medicinal chemistry filters, including the BMS, Dundee, Glaxo, and Inpharmatica rules, as well as the Pan-Assay Interference Compounds (PAINS) filter set. The resulting curated small molecule library therefore represented a collection of small, synthetically accessible, and medicinally relevant scaffolds poised for the subsequent virtual screening campaign.

4.4. Virtual Screening and Hit Identification

To identify novel and potent chemical scaffolds, a de novo design strategy was employed using the CReM-dock software [39] in its "Hit generation" mode. The process was initiated with a library containing 27,053 chemical small molecule. In a fully automated and iterative workflow, these small molecules were first docked into the prioritized ICP0 target pocket using the AutoDock Vina algorithm. The protonation states of all molecules were assigned at a physiological pH using molgpka, and all docking parameters were specified in a dedicated Vina configuration file.

Following the initial docking, the most promising molecules were selected as seeds for chemical elaboration. The CReM-dock pipeline then systematically generated new, chemically reasonable molecules by growing and modifying these seeds in subsequent iterations. This generative process was guided by an objective function prioritizing docking efficiency, ensuring that each new generation of molecules was progressively optimized for binding. Throughout the campaign, defined thresholds for key physicochemical parameters were enforced to maintain drug-like properties in the generated compounds. This entire high-throughput process was executed in parallel on a 32-core system. The final output was a set of novel, optimized molecules, ranked by their predicted binding affinity (ΔG in kcal/mol), which served as high-quality "hits" for the subsequent design of bivalent degraders.

4.5. Hit Elaboration and Bivalent Degrader Design

Following the identification of novel chemical scaffolds, a focused, structure-based approach was employed to construct the final bivalent degrader. The single, top-ranked small molecule hit from the generative design process was selected to serve as the "warhead" for the chimera. A structural model of a functionally critical ICP0 dimer, encompassing residues 1–388 and thus including both the RING finger and PML degradation domains, was generated using the Chai-1 AI-driven protein structure prediction platform. Two copies of the selected warhead were then docked into the two identical target pockets on this dimer model using AutoDock Vina to determine their optimal binding poses. To construct the final bivalent degrader, the 16-carbon alkyl linker was computationally attached at the C11 carbon of the Hit 7 warhead scaffold. As shown in the 2D interaction diagram, this site was determined to be the optimal anchor point. This linker attachment site allows the linker to extend towards the second protomer without interfering with the critical hydrogen bond between the warhead and the side chain of Glu112, thus preserving the key interaction that anchors the molecule in the binding pocket. This procedure yielded a single, rationally designed bivalent degrader, and the resulting model of its ternary complex (ICP0–Degrader–ICP0) was advanced for further evaluation.

4.6. ADMET Prediction

To ensure the selection of a high-quality starting point and to characterize the final candidate, a multi-stage ADMET analysis was performed. First, the initial pool of generated small molecule hits was evaluated for drug-like properties, allowing us to select the top-ranked scaffold for elaboration based on both its binding affinity and its favorable physicochemical characteristics.

Subsequently, the single, final bivalent degrader was assessed for its predicted ADMET (Absorption, Distribution, Metabolism, Excretion, and Toxicity) profile. This characterization was performed using the SwissADME and Deep-PK web servers. A comprehensive set of parameters was evaluated, including predicted aqueous solubility (LogS), blood–brain barrier permeability (LogBB), and potential toxicological flags like the AMES test. This final analysis served to characterize our sole lead candidate and confirm its suitability before proceeding with more rigorous validation.

4.7. Structural Visualization

Three-dimensional representations of proteins and complexes shown in the Figures 2 and 3 were visualized and rendered using UCSF Chimera v.1.19 [40] and Mol* [41]. Two-dimensional diagrams detailing protein–ligand interactions were generated using the LigPlot+ v.2.2 [42] program.

5. Conclusions

This in silico investigation has described a scalable computational strategy for the rational design of the first-in-class homoPROTAC targeting the essential HSV-1 E3 ligase ICP0. Our workflow, which combines AI-driven structure prediction with an iterative generative design process, successfully identified a superior druggable pocket on ICP0 and yielded a lead candidate, ICP0-deg-01, with structural features predicted to cause the viral ICP0 to self-destruct. This work establishes computational proof-of-concept for a potential new class of antiviral therapeutics designed to address the dual challenge of drug resistance and viral latency. In conclusion, this study represents an example of the convergence of molecular virology and modern computational chemistry. It proposes and provides a model for a paradigm of "viral self-destruction" that could potentially be transferable to other persistent pathogens and suggests a promising new direction for rational antiviral design.

Author Contributions: L.S. conceived the study and designed the computational workflow; L.S., A.S., M.E.S. and Z.B.S. performed the virtual screening and docking calculations; O.A., L.S., F.H.K.B. and S.A. were responsible for data curation and analysis; M.G.K., S.A. and H.B. supervised the project and provided critical insights. All authors contributed to the writing and editing of the manuscript. All authors have read and agreed to the published version of the manuscript.

Funding: This research received no external funding.

Data Availability Statement: The data that supports the findings of this study, including the final protein model and docking results, are available from the corresponding author upon reasonable request.

Conflicts of Interest: The authors declare no conflicts of interest.

Abbreviations

The following abbreviations are used in this manuscript:

HSV-1	Human Herpes Simplex Virus 1
TPD	Targeted Protein Degradation
PROTAC	Proteolysis-Targeting Chimera

UPS	Ubiquitin–Proteasome System
ADMET	Absorption, Distribution, Metabolism, Excretion, and Toxicity
RMSD	Root Mean Square Deviation
ICP	Infected Cell Protein
CYP	Cytochrome P450
pLDDT	predicted Local Distance Difference Test
pTM	predicted TM-score
ipTM	interface pTM
SA Score	Synthetic Accessibility Score
SASA	Solvent-Accessible Surface Area

Appendix A

Appendix A.1

Infected Cell Protein 0 (ICP0) is a central viral regulator that counteracts host defenses by targeting a wide range of cellular proteins. The diagram below illustrates the key host pathways disrupted by ICP0 to promote viral replication and immune evasion.

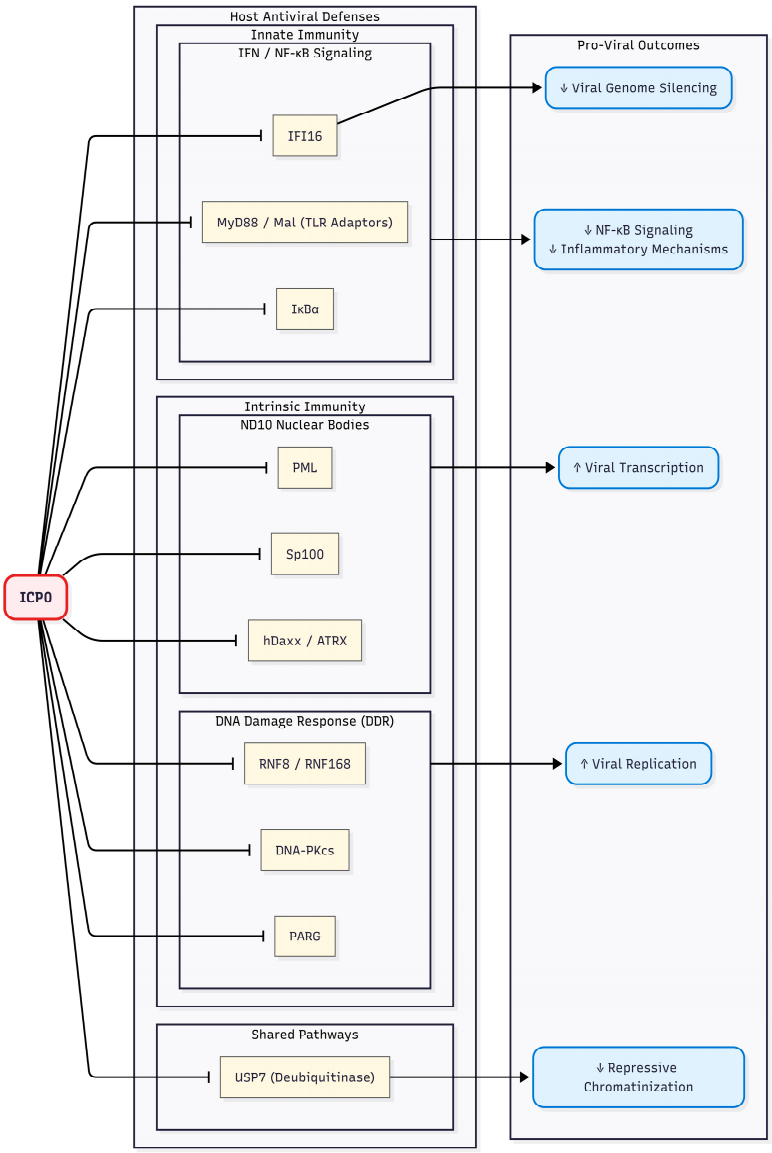


Figure A1. A detailed map of the host proteins and pathways targeted by the HSV-1 protein ICP0. This diagram illustrates the comprehensive strategy ICP0 employs to neutralize host antiviral defenses, thereby promoting viral infection. ICP0 functions as a central hub that systematically dismantles key

components across multiple layers of cellular immunity. Innate and Intrinsic Immunity: ICP0 directly counteracts the cell's primary antiviral responses. It targets core components of the ND10 nuclear bodies, including PML and Sp100, for degradation. This action is critical as it overcomes the host's attempts at viral genome silencing and directly promotes viral transcription. Furthermore, it dismantles innate immune signaling by targeting proteins like IFI16, MyD88, Mal, and IκBα. This targeted disruption blocks pathways that lead to an inflammatory response, such as NF-κB signaling, and prevents the silencing of the viral genome. DNA Damage Response (DDR): The virus also neutralizes the cell's DNA damage response to ensure its own replication is not hindered. ICP0 targets key proteins within this pathway, such as RNF8, RNF168, and DNA-PKcs, an action that ultimately facilitates viral replication. Overall, by degrading this strategic collection of host proteins, ICP0 effectively cripples the cell's defense systems. This creates a cellular environment that is highly permissive for the virus, leading to enhanced viral gene expression, successful replication, and evasion of the host immune response.

Appendix A.2. Structural Model Confidence

The three-dimensional structure of the full-length ICP0 protein was predicted using the Chai-1 AI platform. The confidence of this prediction was assessed using the predicted Local Distance Difference Test (pLDDT) score, which measures the accuracy of local interatomic distances on a scale of 0 to 100.

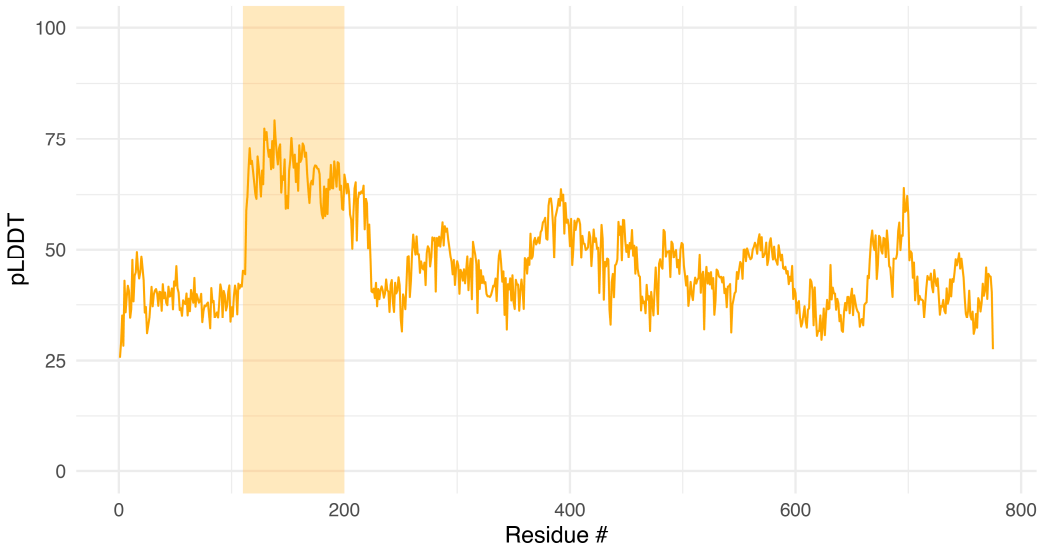


Figure A2. Per-residue confidence score (pLDDT) of the predicted ICP0 structure. The plot shows the pLDDT score for each amino acid residue in the 775-amino-acid sequence of ICP0. While the full-length protein has an average pLDDT of 46.9, the functionally critical region for this study (residues 110–200, highlighted in orange) was predicted with substantially higher confidence, showing a mean pLDDT score of 66.6. This higher local confidence supported its use for subsequent druggability analysis and docking studies.

Appendix A.3. Predicted ADMET Profile of Lead Candidate ICP0-deg-01

The predicted ADMET and physicochemical properties of the final lead candidate, ICP0-deg-01, were calculated to provide an initial assessment of the molecule's drug-like characteristics, as described in Section 4. The results are summarized in Table A1.

Table A1. Predicted physicochemical, pharmacokinetic, and drug-likeness properties for the final lead candidate, ICP0-deg-01.

Property	Predicted Value
Molecular Weight (Da)	1091.34
Consensus LogP	9.84
Topological Polar Surface Area (Å^2)	220.82
Rotatable Bonds	27
Aqueous Solubility (ESOL)	Insoluble (LogS = −12.5)
GI Absorption	Low
Blood–Brain Barrier Permeation	No
P-glycoprotein (Pgp) Substrate	Yes
CYP1A2 Inhibitor	No
CYP2C19 Inhibitor	No
CYP2C9 Inhibitor	No
CYP2D6 Inhibitor	No
CYP3A4 Inhibitor	No
Lipinski Rule of 5 Violations	4
Bioavailability Score	0.17
PAINS Alerts	0
Synthetic Accessibility Score	8.7

References

1. James, C.; Harfouche, M.; Welton, N.J.; Turner, K.M.; Abu-Raddad, L.J.; Gottlieb, S.L.; Looker, K.J. Herpes Simplex Virus: Global Infection Prevalence and Incidence Estimates, 2016. *Bull. World Health Organ.* **2020**, *98*, 315–329. [CrossRef]
2. Su, D.; Han, L.; Shi, C.; Li, Y.; Qian, S.; Feng, Z.; Yu, L. An Updated Review of HSV-1 Infection-Associated Diseases and Treatment, Vaccine Development, and Vector Therapy Application. *Virulence* **2024**, *15*, 2425744. [CrossRef]
3. Riley, G.; Cloete, E.; Walls, T. Challenges of Timely Investigation and Treatment of Neonatal Herpes Simplex Virus Infection. *J. Paediatr. Child Health* **2023**, *59*, 385–388. [CrossRef] [PubMed]
4. Oh, J.J.; Jaggi, U.; Tormanen, K.; Wang, S.; Hirose, S.; Ghiasi, H. The Anti-Apoptotic Function of HSV-1 LAT in Neuronal Cell Cultures but Not Its Function during Reactivation Correlates with Expression of Two Small Non-Coding RNAs, sncRNA1&2. *PLoS Pathog.* **2024**, *20*, e1012307. [CrossRef] [PubMed]
5. Dochnal, S.A.; Krakowiak, P.A.; Whitford, A.L.; Cliffe, A.R. Physiological Oxygen Concentration during Sympathetic Primary Neuron Culture Improves Neuronal Health and Reduces HSV-1 Reactivation. *Microbiol. Spectr.* **2024**, *12*, e02031-24. [CrossRef] [PubMed]
6. Grams, T.R.; Edwards, T.G.; Bloom, D.C. A Viral lncRNA Tethers HSV-1 Genomes at the Nuclear Periphery to Establish Viral Latency. *J. Virol.* **2023**, *97*, e01438-23. [CrossRef]
7. Bautista, L.; Sirimanotham, C.; Espinoza, J.; Cheng, D.; Tay, S.; Drayman, N. A Drug Repurposing Screen Identifies Decitabine as an HSV-1 Antiviral. *Microbiol. Spectr.* **2024**, *12*, e01754-24. [CrossRef]
8. Gosavi, A.A.; Thorat, P.A.; Mulla, J.A.S. Formulation and Evaluation of Acyclovir Loaded Transferosomal Gel for Transdermal Drug Delivery. *J. Drug Deliv. Ther.* **2024**, *14*, 122–130. [CrossRef]
9. Spataro, F.; Ria, R.; Choul, N.; Vacca, A.; Solimando, A.G.; Girolamo, A.D. Acyclovir Desensitization. A Case Report and a Review of Desensitization Strategies. *J. Infect. Dev. Ctries.* **2025**, *19*, 174–180. [CrossRef]
10. Kawsar, S.M.A.; Munia, N.S.; Saha, S.; Ozeki, Y. In Silico Pharmacokinetics, Molecular Docking and Molecular Dynamics Simulation Studies of Nucleoside Analogs for Drug Discovery—A Mini Review. *Mini-Rev. Med. Chem.* **2024**, *24*, 1070–1088. [CrossRef]
11. Liu, S.; Knafels, J.D.; Chang, J.S.; Waszak, G.A.; Baldwin, E.T.; Deibel, M.R.; Thomsen, D.R.; Homa, F.L.; Wells, P.A.; Tory, M.C.; et al. Crystal Structure of the Herpes Simplex Virus 1 DNA Polymerase*. *J. Biol. Chem.* **2006**, *281*, 18193–18200. [CrossRef] [PubMed]
12. Álvarez, D.M.; Castillo, E.; Duarte, L.F.; Arriagada, J.; Corrales, N.; Farías, M.A.; Henríquez, A.; Agurto-Muñoz, C.; González, P.A. Current Antivirals and Novel Botanical Molecules Interfering with Herpes Simplex Virus Infection. *Front. Microbiol.* **2020**, *11*, 139. [CrossRef] [PubMed]
13. Birkmann, A.; Bonsmann, S.; Kropeit, D.; Pfaff, T.; Rangaraju, M.; Sumner, M.; Timmler, B.; Zimmermann, H.; Buschmann, H.; Ruebsamen-Schaeff, H. Discovery, Chemistry, and Preclinical Development of Pritelivir, a Novel Treatment Option for Acyclovir-Resistant Herpes Simplex Virus Infections. *J. Med. Chem.* **2022**, *65*, 13614–13628. [CrossRef] [PubMed]

14. Lv, W.; Zhou, L.; Wu, J.; Cheng, J.; Duan, Y.; Qian, W. Anti-HSV-1 Agents: An Update. *Front. Pharmacol.* **2025**, *15*, 1451083. [CrossRef]
15. Frejborg, F.; Kalke, K.; Hukkanen, V. Current Landscape in Antiviral Drug Development against Herpes Simplex Virus Infections. *Smart Med.* **2022**, *1*, e20220004. [CrossRef] [PubMed]
16. Kuo, J.-Y.; Yeh, C.-S.; Wang, S.-M.; Chen, S.-H.; Wang, J.-R.; Chen, T.-Y.; Tsai, H.-P. Acyclovir-Resistant HSV-1 Isolates among Immunocompromised Patients in Southern Taiwan: Low Prevalence and Novel Mutations. *J. Med. Virol.* **2023**, *95*, e28985. [CrossRef]
17. Zhong, G.; Chang, X.; Xie, W.; Zhou, X. Targeted Protein Degradation: Advances in Drug Discovery and Clinical Practice. *Signal Transduct. Target. Ther.* **2024**, *9*, 308. [CrossRef]
18. Chen, Y.; Liu, F.; Pal, S.; Hu, Q. Proteolysis-Targeting Drug Delivery System (ProDDS): Integrating Targeted Protein Degradation Concepts into Formulation Design. *Chem. Soc. Rev.* **2024**, *53*, 9582–9608. [CrossRef]
19. Xue, Y.; Bolinger, A.A.; Zhou, J. Novel Approaches to Targeted Protein Degradation Technologies in Drug Discovery. *Expert Opin. Drug Discov.* **2023**, *18*, 467–483. [CrossRef]
20. Ambrozkiewicz, M.C.; Cuthill, K.J.; Harnett, D.; Kawabe, H.; Tarabykin, V. Molecular Evolution, Neurodevelopmental Roles and Clinical Significance of HECT-Type UBE3 E3 Ubiquitin Ligases. *Cells* **2020**, *9*, 2455. [CrossRef]
21. Pan, B.; Mountford, S.J.; Kiso, M.; Anderson, D.E.; Papadakis, G.; Jarman, K.E.; Tilmanis, D.R.; Maher, B.; Tran, T.; Shortt, J.; et al. Targeted Protein Degraders of SARS-CoV-2 Mpro Are More Active than Enzymatic Inhibition Alone with Activity against Nirmatrelvir Resistant Virus. *Commun. Med.* **2025**, *5*, 140. [CrossRef] [PubMed]
22. Borges, P.H.O.; Ferreira, S.B.; Silva, F.P. Recent Advances on Targeting Proteases for Antiviral Development. *Viruses* **2024**, *16*, 366. [CrossRef]
23. McCloskey, E.; Kashipathy, M.; Cooper, A.; Gao, P.; Johnson, D.K.; Battaile, K.P.; Lovell, S.; Davido, D.J. HSV-1 ICP0 Dimer Domain Adopts a Novel β-Barrel Fold. *Proteins Struct. Funct. Bioinform.* **2024**, *92*, 830–841. [CrossRef]
24. Perusina Lanfranca, M.; van Loben Sels, J.M.; Ly, C.Y.; Grams, T.R.; Dhummakupt, A.; Bloom, D.C.; Davido, D.J. A 77 Amino Acid Region in the N-Terminal Half of the HSV-1 E3 Ubiquitin Ligase ICP0 Contributes to Counteracting an Established Type 1 Interferon Response. *Microbiol. Spectr.* **2022**, *10*, e00593-22. [CrossRef]
25. Harrell, T.L.; Davido, D.J.; Bertke, A.S. Herpes Simplex Virus 1 (HSV-1) Infected Cell Protein 0 (ICP0) Targets of Ubiquitination during Productive Infection of Primary Adult Sensory Neurons. *Int. J. Mol. Sci.* **2023**, *24*, 2931. [CrossRef]
26. Jan Fada, B.; Guha, U.; Zheng, Y.; Reward, E.; Kaadi, E.; Dourra, A.; Gu, H. A Novel Recognition by the E3 Ubiquitin Ligase of HSV-1 ICP0 Enhances the Degradation of PML Isoform I to Prevent ND10 Reformation in Late Infection. *Viruses* **2023**, *15*, 1070. [CrossRef]
27. Hou, F.; Sun, Z.; Deng, Y.; Chen, S.; Yang, X.; Ji, F.; Zhou, M.; Ren, K.; Pan, D. Interactome and Ubiquitinome Analyses Identify Functional Targets of Herpes Simplex Virus 1 Infected Cell Protein 0. *Front. Microbiol.* **2022**, *13*, 856471. [CrossRef] [PubMed]
28. Das, R.; Hembram, D. The Viral SUMO-Targeted Ubiquitin Ligase ICP0 Is Phosphorylated and Activated by Host Kinase Chk2. *FASEB J.* **2021**, *35*, 1952–1977. [CrossRef]
29. Perusina Lanfranca, M.; Mostafa, H.H.; Davido, D.J. HSV-1 ICP0: An E3 Ubiquitin Ligase That Counteracts Host Intrinsic and Innate Immunity. *Cells* **2014**, *3*, 438–454. [CrossRef]
30. Rodríguez, M.C.; Dybas, J.M.; Hughes, J.; Weitzman, M.D.; Boutell, C. The HSV-1 Ubiquitin Ligase ICP0: Modifying the Cellular Proteome to Promote Infection. *Virus Res.* **2020**, *285*, 198015. [CrossRef]
31. Maillet, S.; Naas, T.; Crepin, S.; Roque-Afonso, A.-M.; Lafay, F.; Efstathiou, S.; Labetoulle, M. Herpes Simplex Virus Type 1 Latently Infected Neurons Differentially Express Latency-Associated and ICP0 Transcripts. *J. Virol.* **2006**, *80*, 9310–9321. [CrossRef]
32. Zografou-Barredo, N.A.; Hallatt, A.J.; Goujon-Ricci, J.; Cano, C. A Beginner's Guide to Current Synthetic Linker Strategies towards VHL-Recruiting PROTACs. *Bioorg. Med. Chem.* **2023**, *88–89*, 117334. [CrossRef]
33. The UniProt Consortium. UniProt: The Universal Protein Knowledgebase in 2025. *Nucleic Acids Res.* **2025**, *53*, D609–D617. [CrossRef]
34. Abramson, J.; Adler, J.; Dunger, J.; Evans, R.; Green, T.; Pritzel, A.; Ronneberger, O.; Willmore, L.; Ballard, A.J.; Bambrick, J.; et al. Accurate Structure Prediction of Biomolecular Interactions with AlphaFold 3. *Nature* **2024**, *630*, 493–500. [CrossRef] [PubMed]
35. Passaro, S.; Corso, G.; Wohlwend, J.; Reveiz, M.; Thaler, S.; Somnath, V.R.; Getz, N.; Portnoi, T.; Roy, J.; Stark, H.; et al. Boltz-2: Towards Accurate and Efficient Binding Affinity Prediction. *bioRxiv* **2025**. [CrossRef]
36. Discovery, C.; Boitreaud, J.; Dent, J.; McPartlon, M.; Meier, J.; Reis, V.; Rogozhnikov, A.; Wu, K. Chai-1: Decoding the Molecular Interactions of Life. *bioRxiv* **2024**. [CrossRef]
37. Team, B.A.A.; Chen, X.; Zhang, Y.; Lu, C.; Ma, W.; Guan, J.; Gong, C.; Yang, J.; Zhang, H.; Zhang, K.; et al. Protenix—Advancing Structure Prediction Through a Comprehensive AlphaFold3 Reproduction. *bioRxiv* **2025**. [CrossRef]
38. Baek, M.; Anishchenko, I.; Humphreys, I.R.; Cong, Q.; Baker, D.; DiMaio, F. Efficient and Accurate Prediction of Protein Structure Using RoseTTAFold2. *bioRxiv* **2023**. [CrossRef]

39. Minibaeva, G.; Polishchuk, P. CReM-Dock: De Novo Design of Synthetically Feasible Compounds Guided by Molecular Docking. *ChemRxiv* **2024**. [CrossRef]
40. Pettersen, E.F.; Goddard, T.D.; Huang, C.C.; Couch, G.S.; Greenblatt, D.M.; Meng, E.C.; Ferrin, T.E. UCSF Chimera—A Visualization System for Exploratory Research and Analysis. *J. Comput. Chem.* **2004**, *25*, 1605–1612. [CrossRef]
41. Sehnal, D.; Bittrich, S.; Deshpande, M.; Svobodová, R.; Berka, K.; Bazgier, V.; Velankar, S.; Burley, S.K.; Koča, J.; Rose, A.S. Mol* Viewer: Modern Web App for 3D Visualization and Analysis of Large Biomolecular Structures. *Nucleic Acids Res.* **2021**, *49*, W431–W437. [CrossRef] [PubMed]
42. Laskowski, R.A.; Swindells, M.B. LigPlot+: Multiple Ligand–Protein Interaction Diagrams for Drug Discovery. *J. Chem. Inf. Model.* **2011**, *51*, 2778–2786. [CrossRef] [PubMed]

Disclaimer/Publisher's Note: The statements, opinions and data contained in all publications are solely those of the individual author(s) and contributor(s) and not of MDPI and/or the editor(s). MDPI and/or the editor(s) disclaim responsibility for any injury to people or property resulting from any ideas, methods, instructions or products referred to in the content.